Received: 24 September 2025 | Revised: 2 December 2025 | Accepted: 25 December 2025 | Published online: 13 January 2026

RESEARCH ARTICLE

Artificial Intelligence and Applications
2026, Vol. 00(00) 1-10
DOI: 10.47852/bonviewAIA62027747

BON VIEW PUBLISHING

A New Domain-Independent Approach for Classification of Bacteria, Fungus, and Virus-Infected Fruit and Leaf Images

Poornima Basatti Hanuma Gowda[1], Basavanna Mahadevappa[1,*], Shivakumara Palaiahnakote[2,3], Muhammad Hammad Saleem[2,3] and Niranjan Mallappa Hanumanthu[4]

[1] *Department of Studies in Computer Science, Davangere University, India*

[2] *School of Science, Engineering, and Environment, University of Salford, UK*

[3] *Data Science and Artificial Intelligence Hub, University of Salford, UK*

[4] *Department of Studies in Biotechnology, Davangere University, India*

Abstract: Early and reliable detection of bacterial, fungal, and viral infections in fruits and leaves is essential for improving crop productivity, preventing disease spread, and supporting food security. Most existing approaches are domain-specific and struggle to generalize across diverse plant organs or varying image qualities. To address this challenge, we propose a novel domain-independent classification framework that integrates quality-metric features—Mean Squared Error (MSE), Peak Signal-to-Noise Ratio (PSNR), and Structural Similarity Index (SSIM)—with an adapted lightweight Convolutional Neural Network (CNN). This is the first approach that explores quality measures as features for addressing challenges of classification of fruits and leaves infected by virus, fungus, and bacteria. The method first performs connected-component analysis on K-means clusters generated from R, G, B, and Gray channels to isolate disease-relevant regions and extract quality-based features. These features are fused with visual features extracted from the RGB images using a multimodal CNN architecture. Extensive experiments conducted on the proposed fruit–leaf dataset and four external benchmark datasets demonstrate that the model achieves high accuracy, strong robustness to blur, noise, rotation, and scaling, and superior generalization performance compared with state-of-the-art methods. Cross-domain evaluations further confirm that the proposed method is domain-independent and reliable for the classification of fruits and leaves infected by bacteria, fungi, and viruses.

Keywords: connected component labeling, quality measures, convolutional neural networks, fruit/leaf disease classification

1. Introduction

Adverse environmental conditions often lead to fruits and leaves being affected by bacterial and fungal diseases. Diseases affecting fruits and leaves reduce agricultural production worldwide, causing significant economic losses and compromising food security. Traditional diagnostic methods based on visual inspection are limited to human observation, expertise, and resources. Rapid developments in digital imaging technologies and machine learning algorithms have provided promising solutions to overcome these challenges. Image-based disease detection technology has become a powerful method for non-invasive, rapid, and accurate disease detection [1]. Bacterial, viral, and fungal pathogens are the main pathogens, each presenting diagnostic challenges. These diseases can lead to crop loss, and their symptoms are often subtle and difficult to distinguish through visual inspection alone. Therefore, the identification of images infected by bacteria, viruses, and fungi is difficult and important for assessing crop health and productivity.

Methods have been proposed in the literature for identifying viral, bacterial, and fungal diseases in fruit and leaf images [2]. However, most of these methods focus on specific diseases and fruit or leaf types. Consequently, the ability of state-of-the-art techniques to classify infected images is generally limited. Thus, the classification of diseased fruit and leaf images, irrespective of the types of fruits and leaves (domain-independent), remains a challenge. Simultaneously, the classification of such images can help choose an appropriate method to reduce crop loss and prevent its spread, which makes a significant difference.

Therefore, this study focused on developing a robust and domain-independent system for viral, bacterial, and fungal fruit and leaf image classification. The effects of viruses, bacteria, and fungi are the same regardless of the fruit and leaves. For instance, black spots and white and yellow patches indicate bacterial, fungal, and viral infections. We believe that the image quality changes due to black spots, yellow, and white patches introduced by bacteria, viruses, and fungal diseases. The change is demonstrated by the sample images in Figure 1, where one can see changes in quality in terms of texture and color. This observation motivated us to introduce quality measures as features in the R, G, B, and Gray color spaces for classification. The measures are the Mean Squared Error (MSE), Peak Signal-To-Noise Ratio (PSNR), and Structural Similarity (SSIM). Similarly, a Convolutional Neural Network (CNN) was proposed for encoding quality measure-based features for the classification of images of different diseased fruits and leaves, motivated by the achievements of CNNs in the literature [3]. To enhance the classification performance, the proposed method inputs the

***Corresponding author:** Basavanna Mahadevappa, Department of Studies in Computer Science, Davangere University, India. Email: basavanna.m@davangereuniversity.ac.in

Figure 1
Example images of fruits and leaves infected by bacteria, fungus, and viruses

original images of R, G, B, and Gray to the CNN, along with quality metric-based features.

Therefore, the contributions of this study are as follows: (i) Proposing a simple and effective method for tackling a complex problem is original. (ii) Extracting quality measures as features from various color spaces based on quality differences in disease images is novel compared to current methods. (iii) Adapting a convolutional neural network to combine image features and quality measures for accurate classification is new. The rest of this paper is organized as follows. In Section 2, techniques for identifying fruit and leaf diseases are reviewed. Section 3 describes the CNN and feature extraction processes for classifying bacteria, viruses, and fungal pathogens in fruit and leaf images. Section 4 discusses the results of the classification validation and the robustness of the proposed method. An overview of the proposed approach and future directions is provided in Section 5.

2. Related Work

Based on the type of input data and disease-causing agent, the latest deep learning approaches can be categorized into three main groups: fruit and leaf disease classification, combined fruit and leaf disease classification, and pathogen-specific classification of bacterial, fungal, and viral infections. Early studies on automated plant disease recognition relied on classical image processing and machine learning techniques before the widespread adoption of deep learning-based frameworks [4, 5].

2.1. Fruit disease classification

Sultana et al. [6] developed XAI-FruitNet, an explainable model for fruit classification that enhances interpretability but focuses on fruit quality rather than pathogen type. Bansal et al. [7] presented a CNN-based model for apple disease classification, which showed strong results but was constrained to specific apple diseases only. Anim-Ayeko et al. [8] proposed a deep learning system for blight detection in potato and tomato, which is effective but disease-specific. A study conducted by Mallikarjuna et al. [9] used deep learning for feature extraction and classification using gradient-directional information to improve photos to classify illnesses in areca nuts. Furthermore, Javidan et al. [10] introduced variations in illumination, background clutter, and image quality have been reported to significantly affect fruit disease classification accuracy, highlighting the importance of robust feature learning. Overall, existing methods perform well on specific fruit datasets, but their scope is limited to a particular domain.

2.2. Leaf disease classification

Chandrashekar et al. [11] introduced a Modified Dense Convolution Network (MDCN), for mango leaf disease classification, showing high performance but limited to mango leaf cases. Li et al. [12] proposed a dual-network approach integrating a Multi-fusion U-Net with an enhanced VGG-19 to detect grape leaf diseases in diverse environmental conditions. Liu et al. [13] introduced a flooding-based MobileNet to identify cucumber leaf diseases under natural settings, emphasizing background complexity. Li et al. [14] developed DAC-YOLOv4 for strawberry disease detection. Liu et al. [15] proposed MCDCNet, which utilizes feature fusion and dual-constrained deformable convolution for apple leaf disease detection. Thakkar et al. [16] introduced multi-level feature fusion strategies in CNN-based architectures have also been shown to improve discrimination between visually similar leaf diseases. Thai et al. [17] introduced FormerLeaf, a transformer-based model for cassava leaf disease recognition, which used sparse matrix operations to improve efficiency. Pradhan et al. [18] proposed an involutional neural network for classifying diseases in leaf images, including various pathogens. Rani et al. [19] applied feature-based deep learning for identifying infected leaves. Jiang et al. [2] enhanced CNNs for real-time apple leaf disease detection. In summary, these models offer strong performance for leaf disease tasks; however, their scope is confined to leaf diseases.

2.3. Fruit and leaf disease classification

Vásconez et al. [20] implemented CNN models to detect bacterial wilt in tomatoes, with Xception and MobileNet-v2 showing the best results. Prajwala et al. [3] proposed a method for pomegranate disease detection in both fruit and leaf images using adaptive histogram-based features and an artificial neural network (ANN) classifier. Chin et al. [21] compared deep learning models across several plant disease datasets. Khanal et al. [22] developed a mobile application integrating CNNs for paddy disease detection. Benfenati et al. [23] applied unsupervised deep learning for automatic disease detection in both fruit and leaf images. Most of these approaches are designed for limited plant organs or controlled datasets and struggle to generalize across different domains such as fruits and leaves affected by multiple disease types [24]. In summary, these approaches primarily focus on one or two plant parts and do not comprehensively address all three diseases in plants.

2.4. Virus, bacteria, and fungal disease classification

Cao et al. [25] and Liu and Wang [1] reviewed the challenges and strategies for plant disease detection, including fungal and bacterial infections. Pacal et al. [26] provided comprehensive reviews and case studies on fungal, bacterial, and viral classification using deep models. Tejaswini et al. [27] addressed early detection using CNNs and AI-enhanced feature engineering. Pandian et al. [28] used CNNs for pathogen-infected plant image classification. Wang et al. [29], Thakur et al. [30], and Kumar et al. [31] utilized advanced CNNs and attention-based models to identify multiple pathogens, including viruses, bacteria, and fungi, in various environmental settings. Saraswat et al. [32] proposed a modified deep neural network combined with DSURF features for fungi-bacterial detection. In summary, most of the above methods work well for a particular domain but not for multiple domains simultaneously. Therefore, these methods may not perform well in detecting fruit and leaf diseases.

In conclusion, although recent studies have proposed a range of deep learning models tailored to specific datasets and disease types,

Figure 2
Block diagram of the proposed method

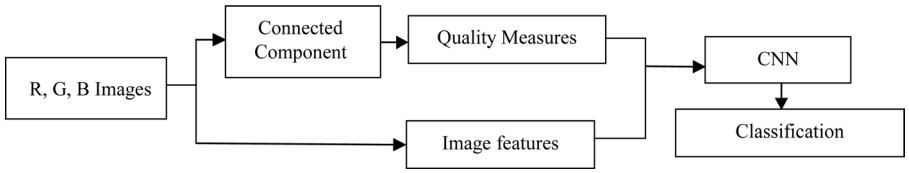

none provide a unified, robust solution for classifying both fruit and leaf images infected by bacterial, fungal, and viral diseases under varying image qualities and conditions. This research gap underscores the need for a domain-independent disease classification framework capable of maintaining consistent performance across diverse plant organs and infection types [33]. A domain-independent model effectively integrates quality metrics and image-based features to achieve reliable and stable results.

3. The Proposed Approach

As noted in the previous section, the classification of fruit and leaf images from viruses, bacteria, and fungi is a complex problem because of the diverse nature of the images. One of the co-authors, a biotechnology expert, observed that bacterial, viral, and fungal infections resulted in black spots, white patches, and yellow patches, respectively. In addition, these infections alter the quality of the images [3, 9]. These findings motivated us to use quality metrics as classification features in this study, specifically MSE, PSNR, and SSIM. To implement quality measure-based features, the proposed method performs a connected component operation to detect the patches in the image as components. Simultaneously, the color of the patches and the input image provide vital cues for the classification of diseased fruit and leaf images. This intuition motivated us to introduce a conventional neural network for fusing images and quality measure-based features for classification. A block diagram of the proposed method is presented in Figure 2. Owing to the simple adapted CNN and handcrafted features, the proposed method is a lightweight model that does not require a large number of training samples and computations, unlike recent heavy deep learning models such as ResNet, DenseNet, and Vision Transformers. In addition, because the problem is new and a larger number of samples are not available for training and experimentation, we believe that the combination of handcrafted features and the adapted lightweight CNN is a better option for classification.

To show that the infection of diseases can change the quality of images arbitrarily, we estimated the BRISQUE and NIQUE non-parametric quality measures for the samples of fruit and leaf diseases, as illustrated in Figures 3 and 4. As shown in Figures 3 and 4, the BRISQUE and NIQUE report arbitrary values, whereas the same measures report almost similar values for healthy images. The black dots, yellow, and white patches affect the image quality.

3.1. Connected components for estimating quality measures

The proposed approach divides an input color image into R, G, B, and Gray channels before using K-means clustering with K = 2 for each color space to produce high and low mean clusters. The value of K is determined empirically. Because of the unsupervised nature of K-means clustering, the mean of the clusters was calculated. The cluster with the highest mean is referred to as a high-contrast cluster, whereas the other cluster is referred to as a low-contrast one. For the sample images shown in Figure 5(a), the detection of connected components in high- and low-contrast clusters for the images of bacterial, fungal, and viral illnesses is shown in Figure 5(b).

Figure 3
Average BRISQUE scores for healthy and diseased fruit and leaf images across the proposed and two benchmark datasets

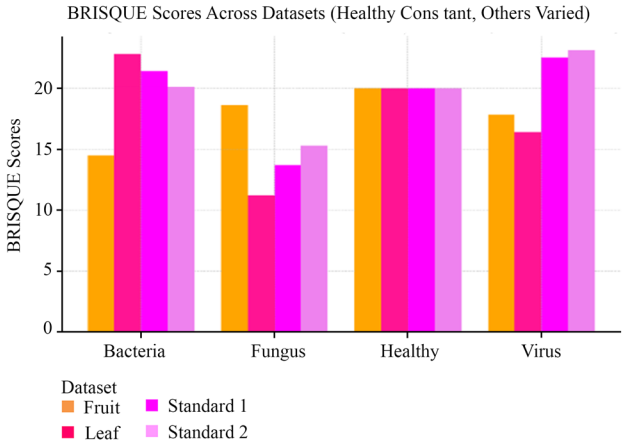

Figure 4
Average NIQE scores for healthy and diseased fruit and leaf images across the proposed and two benchmark datasets

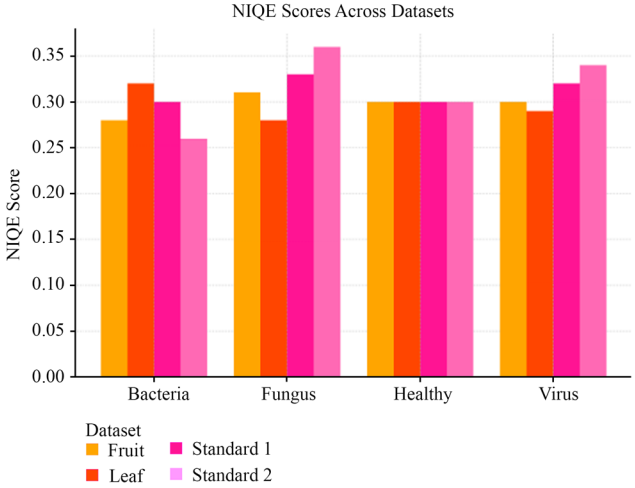

Figure 5 illustrates that for the R, G, B, and Gray spaces, the pixels representing white patches are classified into high mean clusters, while the pixels that represent black spots are classified as low-contrast clusters. The same is not true for pixels that represent yellow patches because some pixels can be classified as high-contrast, and other parts of the yellow patches can be classified as low-contrast clusters. This is because high pixel values represent white patches, low pixel values represent black spots, and neither high nor low pixel values represent yellow patches in the images. The same conclusions can be drawn for the images of the leaves.

Figure 5
Connected components are detected for the infected fruit images

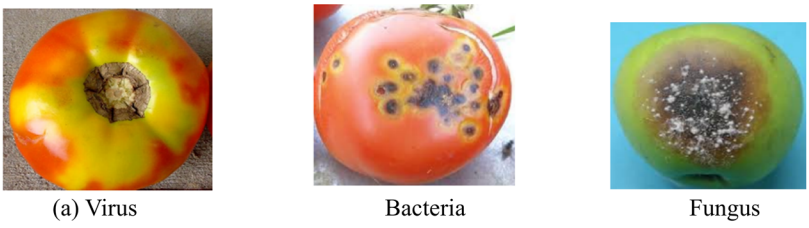

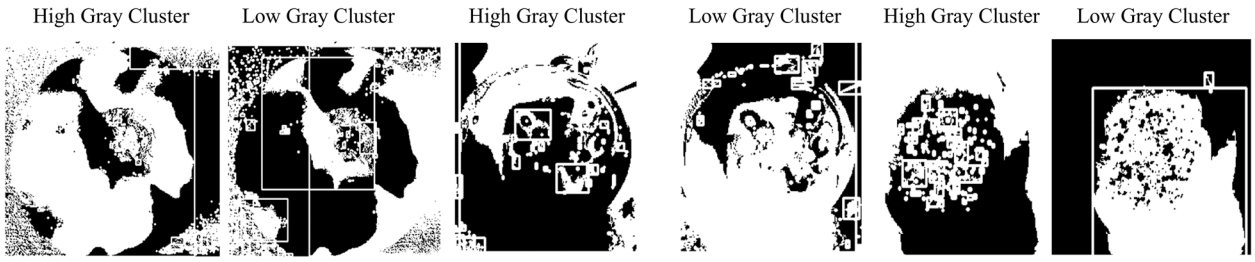

(b) Connected components detection in the high and low mean clusters of fruit images.

As mentioned above, the value of the K is determined empirically, which is 2. This is because of the following. When we look at the cues of bacteria, fungus, and virus in fruit and leaf samples, the dark, white, and yellow patches represent each disease in both fruits and leaves. This implies that the patches have either high or low pixel values compared to the background pixels, irrespective of diseases and fruits, and leaf samples. For example, the dark patches usually have low values while the white patches have high values. However, the values of yellow patches are inclined to high values compared to background pixels. This observation motivated us to introduce K-means clustering with K = 2, such that it outputs high and low mean clusters containing the patches as connected components. This observation is illustrated in Figure 6(a)-(b), where, for K = 2, we can see distinct clusters for different classes, while the clusters are not clear for K = 2, 3, 4, and 5.

The quality measures are estimated for each connected component in the high- and low-contrast clusters of the R, G, B, and Gray spaces and considered as features for classification. This step detects the region of interest and discards the other regions of interest. Consequently, the problem complexity and computation count are reduced, making the proposed approach both effective and efficient. The pixels in the input images (original images) that match the pixels in the clusters are retrieved to calculate the quality measures (MSE, PSNR, and SSIM) for high- and low-contrast clusters in each R, G, B, and Gray space. Quality measurements were estimated using the input

Figure 6
Determining the feasible K values for the successful classification

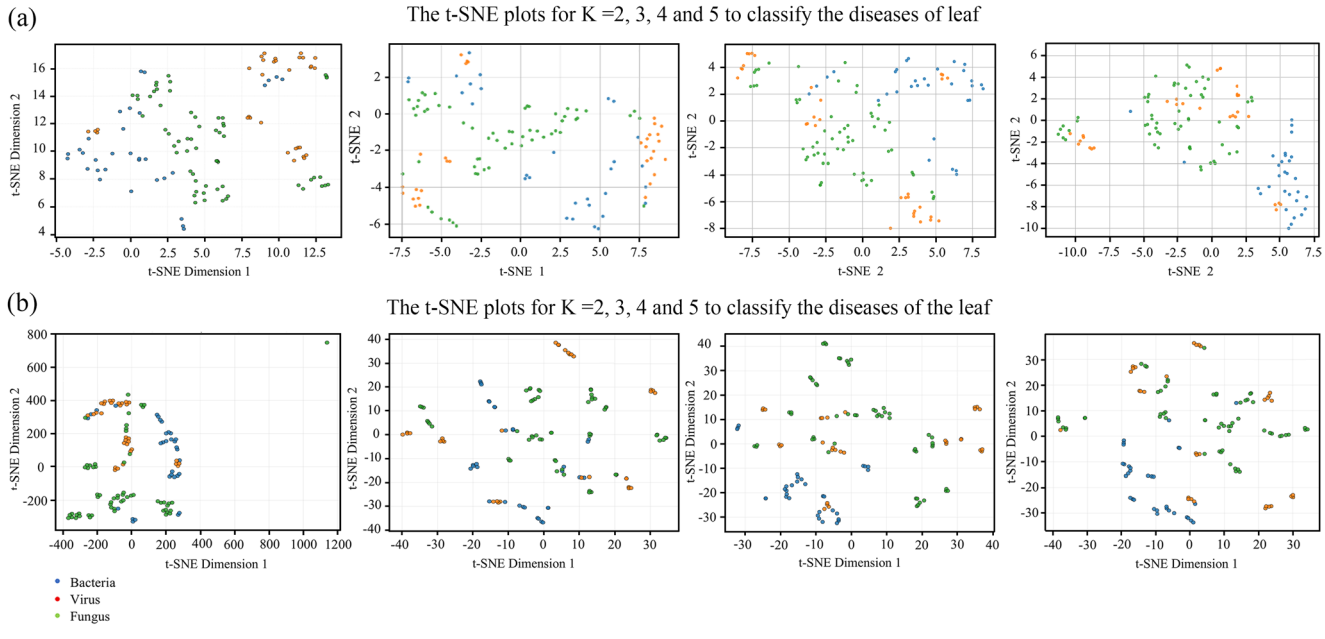

image pixels and clusters. The clusters are considered reconstructed images in this study.

This work uses a gray image in addition to R, G, and B images for connected components extraction. This is because the gray images result in the average of R, G, and B values in the color spaces. This means the gray image can be considered as a normalized image compared to individual R, G, and B images. Therefore, we believe that the features extracted from gray images are robust and stable (this can be confirmed from the results in the Ablation study experiments). The features extracted from the gray image are better than R, G, and B. However, the gray image does not provide color information. This motivated us to extract features from R, G, and B images directly to strengthen the features because color is a key feature for the classification of bacteria, viruses, and fungi. Therefore, the combination of features extracted from gray and R, G, and B separately makes the features robust and generic.

Mean Squared Error (MSE): The average squared difference between the original and reconstructed images is measured by the MSE, as defined in Equation (1).

$$MSE\left(I,I^{'}\right)=\frac{1}{N}\sum_{i=1}^{N}\left(I_i-I^{'}_i\right)^2 \tag{1}$$

where I_i is the pixel value in the original image at pixel ii, I'_i is the pixel value in the reconstructed image at pixel ii, and N represents the total pixel count of the image.

Peak Signal-to-Noise Ratio (PSNR): It is a metric that compares the power of the noise (the difference between the original and compared images) to the greatest power of a signal (an image). It is defined as in Equation (2).

$$PSNR\left(I,I^{'}\right)=20log_{10}\frac{L}{\sqrt{MSE\left(I,I^{'}\right)}} \tag{2}$$

where L is the maximum possible pixel value (for 8-bit images, L = 255) and $MSE\left(I,I^{'}\right)$ is the Mean Squared Error between the original and the compared images.

Structural Similarity Index (SSIM): The SSIM is a perceptual measure of the similarity between two images, considering the brightness, contrast, and structure. It is calculated using Equation (3).

$$SSIM\left(I,I^{'}\right)=\frac{\left(2\mu I\mu I^{'}+C_1\right)\left(2\sigma II^{'}+c_2\right)}{\left(\mu_I^2+\mu_I^2+C_1\left(\sigma_I^2+\sigma_I^2+c_2\right)\right)} \tag{3}$$

where μI and $\mu I^{'}$ are the mean intensities of the original and compared images, respectively. σ_I^2 and $\sigma_{I^{'}}^2$ are the variances of the original and compared images, respectively; and $\sigma I\,I^{'}$ is the covariance between the original and compared images. The division with weak denominators is stabilized by the constants C_1 and C_2.

The average of the features taken from the high-mean and low-mean clusters of the corresponding R, G, B, and Gray images was calculated using the suggested approach. Twelve features in total—three features with four color spaces—are extracted. A convolutional neural network uses these properties to classify data. Figures 7 and 8 illustrate the distributions of the MSE, PSNR, and SSIM for diseased fruit and leaf, where we can see a unique distribution for each class. This demonstrates that the proposed features can successfully classify diseased fruit and leaf images.

3.2. Classification of fruit and leaf images caused by virus, bacteria, and fungus

As noted in the previous section, the extracted quality measures can differentiate between the three diseases. However, a quality metric

Figure 7
The unique feature distribution for the classification of diseased fruit images

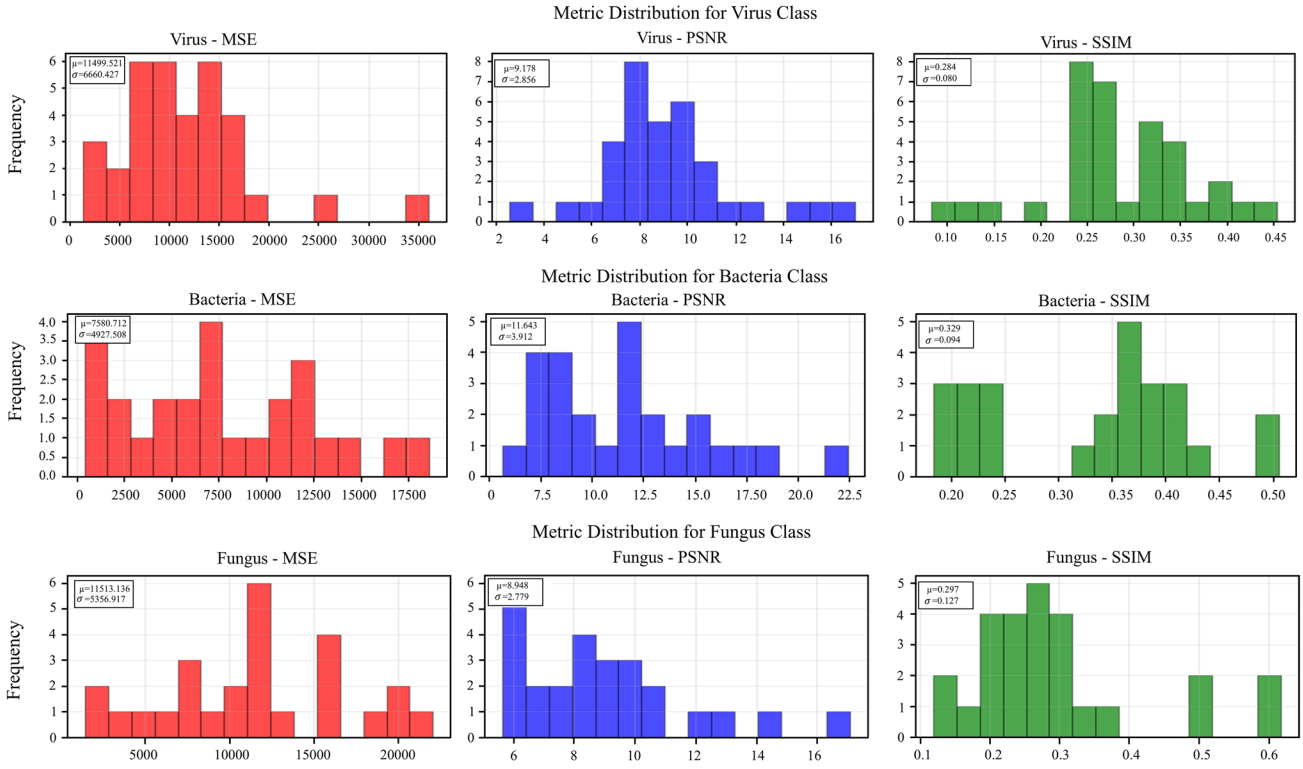

Figure 8
The unique feature distribution for classification of diseased leaf images

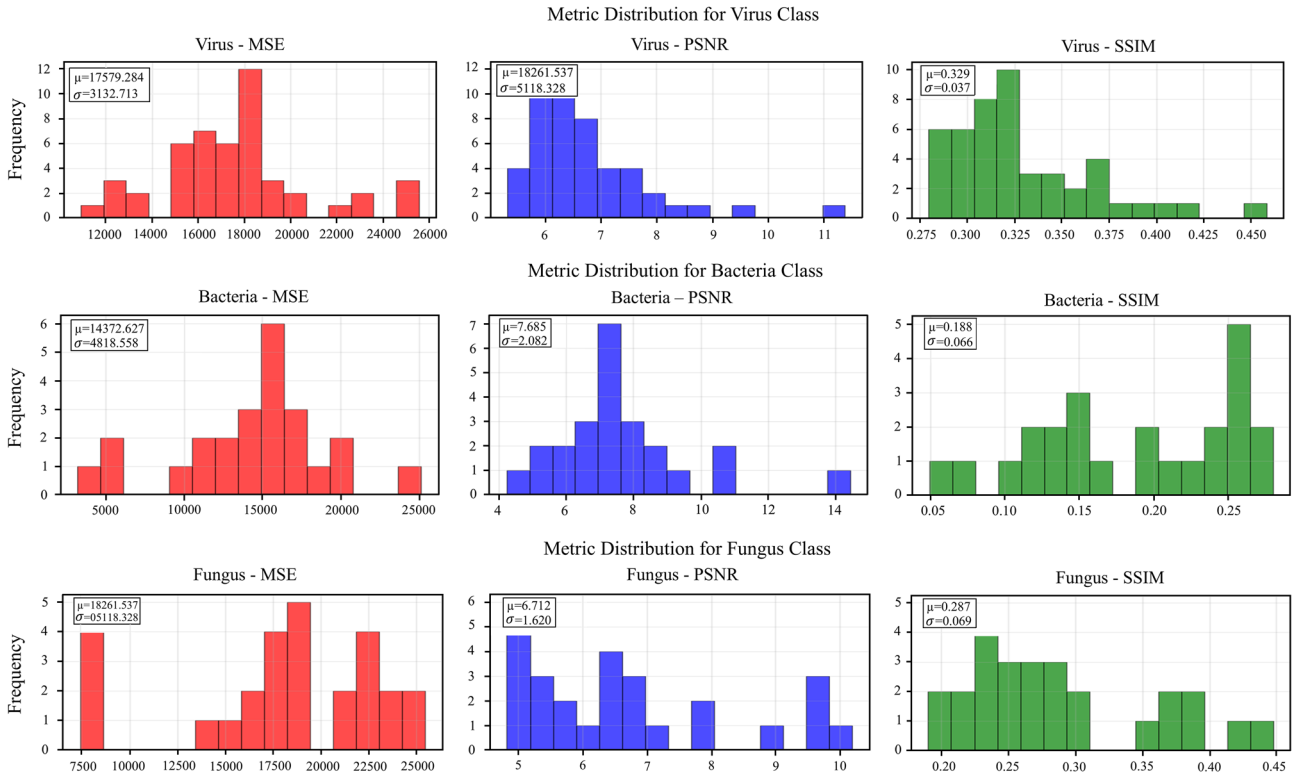

feature alone is insufficient to achieve a high classification rate owing to the multiple domains. Therefore, to improve the classification performance, the input images of R, G, B, and Gray are fed to the CNN along with the quality metric features, as shown in Figure 9.

For each of the R, G, B, and Gray channels, the proposed method obtains connected components from high- and low-mean clusters of the input images as discussed earlier. Three quality metrics were computed for each component in each cluster of the four-color channels. This resulted in 12 features (3 metrics × 4 color spaces) per image, which were normalized and fed into the CSV input branch of the network. The full RGB image (size: 180 × 240 × 3) was directly passed into the CNN branch of the network. Furthermore, both the image (RGB) and extracted features were fused using a concatenation approach for classification. Full RGB and Gray images are processed through a series of convolutional layers in a CNN. These layers extract high-level visual features, such as texture, shape, and spatial patterns. The final output from this branch is a compact visual representation vector after global average pooling and a dense transformation. The outputs of the two branches, the visual features from the CNN, and the structural features from the quality metric, were concatenated into a single unified feature vector. This concatenated representation captures visual and abrupt changes using quality metrics, providing complementary information. The fused feature vector is passed through additional dense layers with dropout for regularization and is finally classified using a SoftMax layer into the respective disease categories (bacteria, fungus, and virus). More details of the classification architecture are presented below.

A multi-channel CNN architecture was used in this study to handle RGB and grayscale picture inputs concurrently. The network begins with parallel input channels for the Red, Green, Blue, and Gray components, which are fed into a series of Conv2D layers with kernel sizes of 3 × 3. The architectural depth progressively increased through the convolutional layers with expanding filter sizes from 64 to 512 filters, which were interspersed with MaxPooling2D layers for spatial dimension reduction and feature concentration. The network incorporates a hierarchical feature extraction approach in which the initial layers extract basic features, whereas the deeper layers process complex patterns. A GlobalPooling2D layer completes the design, and then a rectified linear unit (ReLU) with a special feature combination stage that implies feature fusion capabilities is used. In addition to processing picture characteristics, the model can handle CSV file inputs, demonstrating its capacity to handle more structured data. Multiple measures, including MSE, PSNR, and SSIM, were used to assess network performance. These metrics make the network particularly well-suited for image classification tasks that require both structural and visual data analysis.

The fusion process involves careful dimensional alignment and integration of two distinct feature representations. The 12 quality-metric features, comprising MSE, PSNR, and SSIM values extracted from R, G, B, and Gray color spaces through connected component analysis, first undergo normalization to ensure consistent scaling. These normalized features are then passed through a dense (fully connected) layer with 64 neurons and ReLU activation, followed by dropout regularization (rate: 0.3–0.5), which transforms the 12-dimensional quality feature vector into a 64-dimensional representation that captures structural degradation patterns caused by disease infections. Simultaneously, the full RGB image (180 × 240 × 3) is processed through the CNN branch, where sequential Conv2D layers with progressively increasing filter sizes (64 to 512) extract hierarchical visual features, followed by GlobalAveragePooling2D for spatial dimension reduction and a dense layer with 64 neurons, producing a 64-dimensional visual feature representation vector. The fusion mechanism operates by concatenating these two 64-dimensional vectors using a concatenate layer, creating a unified 128-dimensional feature vector that synergistically combines both the handcrafted quality-metric features and the learned visual

Figure 9
Architecture of the proposed CNN-based framework with quality-metric feature fusion across multiple color channels

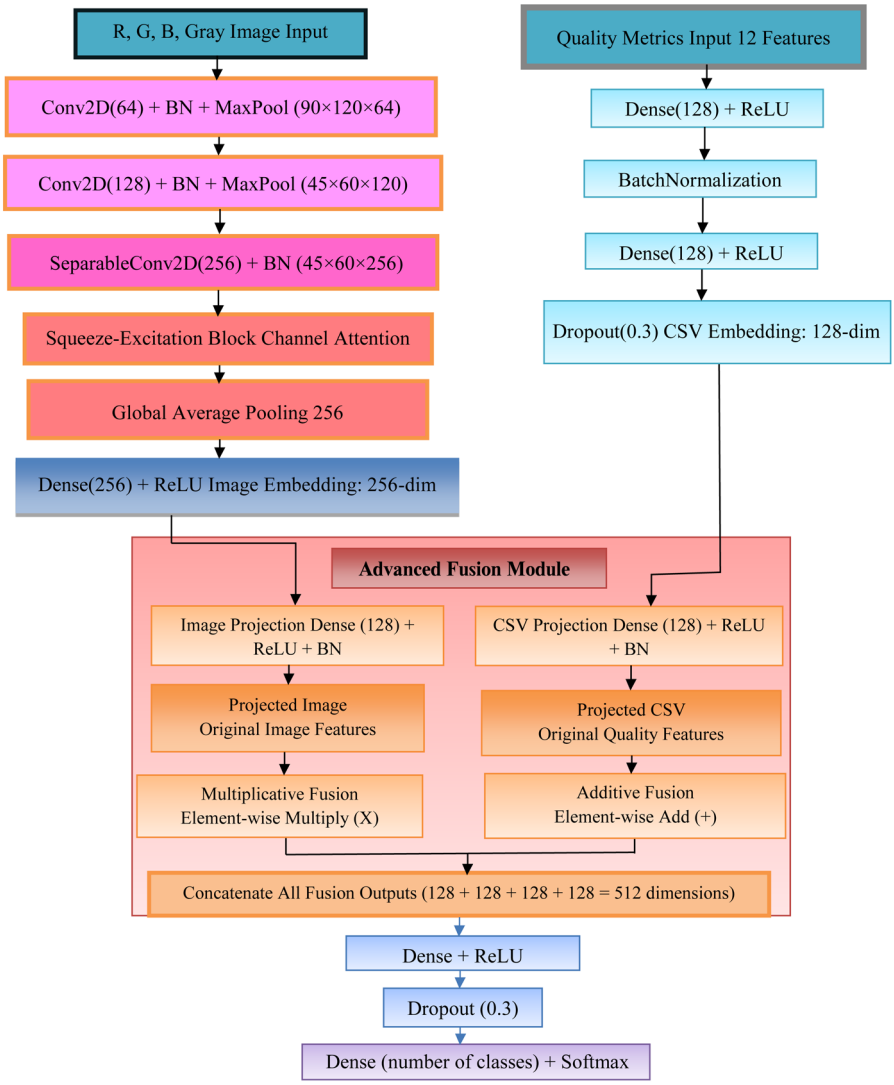

features. The concatenated 128-dimensional vector is then passed through additional dense layers with dropout for regularization before the final softmax classification layer. This fusion strategy at the feature level, rather than at the decision level, enables the model to learn complex interactions between quality degradation patterns and visual disease symptoms to make the proposed method domain-independent for the classification of diverse fruit and leaf disease images.

To ensure consistent feature representation and stable convergence, all extracted quality features (MSE, PSNR, and SSIM) are first normalized before being fed to the CNN. The CNN hyperparameters—kernel sizes (3 × 3), number of filters (64–512), learning rate (1e−4), batch size, and dropout ratios (0.3–0.5)—are determined through an empirical grid-search procedure. Multiple configurations were trained and evaluated using 10-fold cross-validation, and the model achieving the highest validation accuracy was selected as the final configuration. This systematic workflow, beginning with preprocessing → feature normalization → empirical hyperparameter tuning → cross-validation selection, ensures that the parameters remain properly scaled across feature domains and contribute robustly to the final classification performance.

To show the effectiveness of the proposed adapted CNN compared with the baseline CNN, the steps of the baseline and proposed adapted CNN are shown in Figure 10(a) and (b), respectively. In the standard CNN shown in Figure 10(a), the model takes only the raw image input, which passes through a series of convolutional layers (Conv2D), batch normalization, pooling layers (MaxPooling2D), and a final dense layer before classification. This design focuses solely on learning visual patterns from image pixels, such as textures and shapes, without considering other structural cues or image degradation metrics. In contrast, the adapted CNN shown in Figure 10(b) enhances the architecture by introducing a dual branch structure. One branch processes the image input using CNN layers to extract visual features. The second branch takes a set of pre-computed quality metrics (for example, MSE, PSNR, and SSIM from CSV files) as input, which represents the structural degradation in the image caused by the disease itself. These features are processed through a dense layer with dropout to learn high-level representations. The outputs from both the image and quality metric branches were then concatenated (fused) into a combined feature vector, which was passed through additional dense layers for final classification. This fusion mechanism is the core difference: while the standard CNN relies only on raw pixel information, the adopted CNN integrates domain-specific structural features with visual features, making it more robust and accurate for identifying bacterial, fungal, and viral infections across different fruit- and leaf-related domains. This

Figure 10
The proposed adopting CNN vs baseline CNN for the classification of fruit and leaf diseases

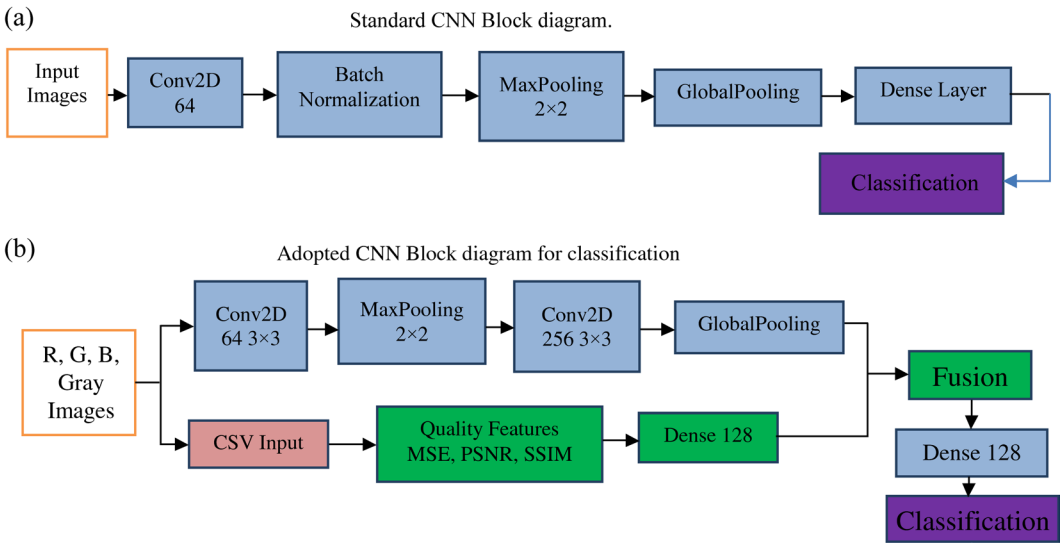

multimodal approach significantly enhances the generalization ability of the model, particularly in cross-dataset scenarios. Figure 11 shows the clusters of different classes obtained for the baseline and proposed adapted CNN. Clusters representing different classes overlap in the case of the baseline CNN, whereas there is no overlap in the case of the modified CNN.

4. Experimental Results

To validate the proposed and current approaches, we collected a dataset from the Biotechnology Department of Davanagere University in Karnataka, India. To discover cures for illnesses, they concentrate on studying bacteria, fungi, and viruses at the microscopic level. However, handling a wide range of images infected with various diseases is challenging because this manual method requires more time and effort. The collected images were verified by experts in the biotechnology department. To make the collection as comprehensive and diverse as possible, images were collected from multiple sources, areas, and fields, open spaces, and under various weather conditions. The proposed approach was also evaluated using two benchmark datasets [34, 35] of images of fruits, plants, leaves, stems, and vegetables affected by bacteria, fungi, and viruses to demonstrate that it is resilient to varying datasets and the number of classes.

4.1. Creation and assessment of datasets

Each class of disease contained 500 images of fruits and leaves; hence, the total dataset size was 1500 for the three classes of fruits and leaves. Images were captured across multiple agricultural fields and experimental settings in Karnataka, India. The dataset will be compiled over six months (July to December 2024). This timeframe allowed for the capture of disease progression under varied climatic conditions. Images were captured with cameras placed approximately 0.5 to 1 meter from the subject to ensure clear visibility of disease symptoms. The camera specifications included 12–24 MP resolutions, standard RGB sensors, and macro lenses for detailed close-up images. A combination of controlled (laboratory settings with plain backgrounds) and uncontrolled (real-world agricultural environments) conditions was used to capture images. Controlled settings ensured high-quality samples for baseline comparisons, whereas uncontrolled environments provided robustness against real-world challenges such as variable lighting, shadows, and occlusions. The dataset incorporated both high-quality and degraded images to simulate real-world conditions. Degradations include blurring, noise, and occlusion by other objects (e.g., leaves and stems). Two datasets containing photos of fruits, plants, stems, and vegetables affected by bacteria, fungi, and viruses were used to test the robustness and generalization capacity of the proposed method [34].

Figure 11
t-SNE distribution for illustrating the effectiveness of the baseline and adapted CNN for classification of fruit and leaf diseases. (a) Clusters of different classes of fruit disease using baseline CNN and adopted CNN for classification, (b) Clusters of different classes of leaf diseases using baseline and adapted CNN for classification

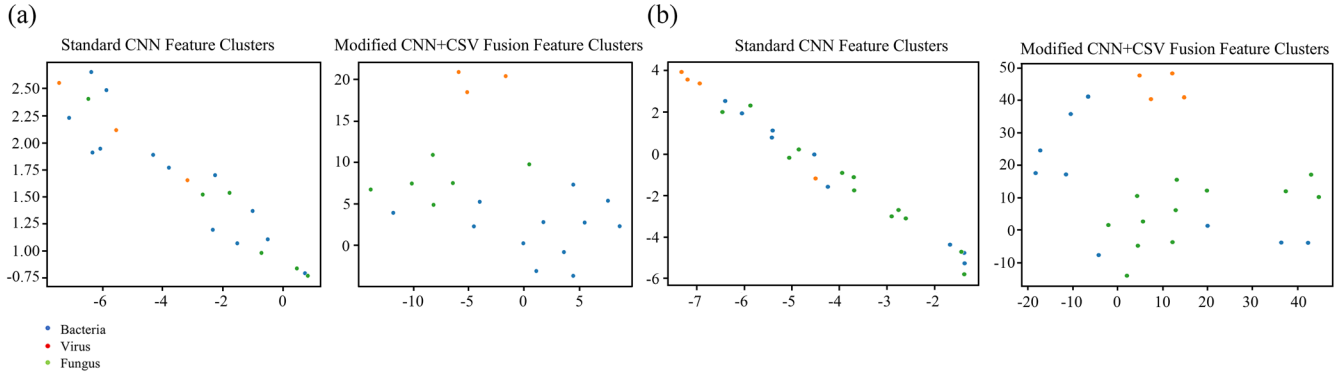

NZDLPlantDisease-v1 dataset: This dataset includes images of kiwifruit, apples, pears, avocados, and grapevines from the agricultural fields of New Zealand. The dataset contains images of multiple diseases on leaves, fruits, and stems, under various environmental conditions. The Bacteria class contained 1500 photographs, the Fungus class 400, the Healthy class 1500 images, and the Viruses class 648 images.

NZDLPlantDisease-v2 dataset: This dataset includes a wide range of photos highlighting plant diseases affecting vegetables grown in New Zealand. The bacteria, fungi, virus, and healthy classes contained 1800, 652, 1800, and 648 images, respectively, for a total of 4900 samples. This includes multiple disease categories that affect different vegetables under various environmental conditions. Consequently, the high accuracy on these benchmark datasets confirms the robustness and capacity for generalization of the proposed method.

Plant Disease Recognition: This dataset provides three classes, namely Healthy, Powdery, and Rust, which have 1382 samples in total. These classes differ from those in our dataset and other standard datasets.

Augmented Grapevine Disease Dataset: This dataset provides four classes of Black Rot, ESCA, Leaf Blight, and Healthy, and each class includes (1,656 original + 1,344 augmented = 3000) 9120 in total. These two datasets differ in terms of diseases, the number of samples for each class, the number of classes, complexities, and applications.

The following state-of-the-art methods were trained and evaluated on our dataset and four benchmark datasets to demonstrate the effectiveness of the proposed model. Using the DenseNet architecture, Chandrashekar et al. [11] created a model for classifying mango leaf diseases without including pathogens. This approach was chosen for the comparative study because its objective was similar to that of the proposed method. Another study, Sultana et al. [6], suggested a model based on the Explainable AI-integrated deep architecture XAI-FruitNet for classifying various fruits. We used the current fruit classification approach [6] for comparative analysis because categorization was the goal of this study. This demonstrates that the general classification method might not be sophisticated enough to categorize photos infected with bacteria, fungi, or viruses. The methods proposed in Du et al. [36] and Linfeng et al. [37] were developed for crop pest disease detection and tomato leaf disease identification, respectively, using deep learning-based models. The methods [25, 30] were implemented to show that the method developed for a specific dataset and disease may not work well for images of multiple domains compared to the proposed method. We estimated a confusion matrix and Average Classification Rate (ACR), which is the mean of the diagonal elements of the confusion matrices, to evaluate the efficacy of the proposed and existing methods. We used 10-fold cross-validation, which automatically selects the number of training and testing samples used. The effectiveness of this approach was confirmed by determining the average of the confusion matrices.

Implementation Details: For our experiments, we employed the following software and hardware components: Software: OS: Windows 10, Editor: VSCODE 1.93, Python: 3.10.12, Optimizer: Adam optimizer, Training Method: Standard supervised learning, Number of Epochs: 3.

Hardware: Processor -AMD Ryzen 3200G @ 3.6GHz, Ram: 8GB, HDD: 1TB. The optimization strategy involved fine-tuning the learning rate (1e−4 to 1e−5), batch size (16, 32), and dropout rates (0.3 to 0.5). The Adam optimizer was used with default momentum parameters ($\beta_1 = 0.9$, $\beta_2 = 0.999$). The final configuration was selected based on validation accuracy using 10-fold cross-validation. This tuning ensured the best convergence and prevented overfitting while maintaining computational efficiency.

4.2. Ablation study

The proposed method, illustrated in Section 3, has vital steps and components for achieving the best classification results. To assess the effectiveness of each component, we conducted ablation experiments, as listed in Table 1. In the proposed work, (i)–(iv) image features are extracted from R, G, B and Gray color spaces; (v) component labeling; (vi)–(viii) quality measures estimated as features; (ix)–(x) high- and low-contrast clusters; and (xi) input images are supplied to CNN directly for classification. The effectiveness of each key step was verified by calculating the average classification rate for the fruit and leaf datasets, as indicated in Table 1. Table 1 shows that all steps contribute to the best results, with the proposed method (xii) achieving the highest average classification rate compared to the individual key steps. The performances of various color spaces were compared, and the green color space contributed more to the classification of fruit and leaf pathogens than the other color spaces. This shows that the green color is effective for images of viruses, bacteria, and fungi. A possible reason for this is that the causes or effects of viruses, bacteria, and fungi can be noticed in green spaces compared to other color spaces. The red and blue spaces may be confused with white and yellow patches caused by fungi and viruses, respectively.

Similarly, when comparing the results obtained with the proposed method without labeling, it can be seen that connected-component labeling is an important step for classification. This is because unnecessary information is filtered out of the image. Similarly, according to the results of the different quality measurements for fruit and leaf data, PSNR was the best measurement for classifying infected fruit and leaf images. This indicates that the PSNR can be applied to images of bacteria, viruses, and fungi. This is because the black spots, white patches, and yellow patches of bacteria, fungi, and viruses are considered to be noisy in the images. Although MSE and SSIM are suitable for identifying similarities between the original and clustered images, they do not contribute significantly to the classification compared to the PSNR-based features.

Additionally, high-contrast clusters can be useful because their contribution to the fruit and leaf data is larger than that of low-contrast clusters when we compare their contributions. This is logical because most pixels represent white patches, and the yellow patches are classified as high-contrast clusters. In other words, high-contrast clusters provide more important information for classification than low-contrast clusters. When the input images were supplied directly to the CNN for classification, the results were not as good as those of the proposed method. Therefore, CNN alone is insufficient for achieving high accuracy. Nonetheless, the outcomes demonstrate that it works well and helps the proposed approach to function better.

Similarly, the contribution of the features and components of the proposed method was validated by adding components one after the

Table 1
ACR of the key steps of the proposed method for fruit and leaf disease classification

SL. no	(i)	(ii)	(iii)	(iv)	(v)	(vi)	(vii)	(viii)	(ix)	(x)	(xi)	(xii)
Steps	Gray	R	G	B	No labeling	MSE	PSNR	SSIM	High-cluster	Low-cluster	Input-CNN	Proposed
Fruit	29.62	33.33	41.48	40.74	57.09	81.82	86.36	72.73	84.88	78.83	56.97	90.81
Leaf	42.86	48.38	49.18	48.38	83.43	76.00	84.00	52.00	91.71	86.76	61.33	95.55

other, as reported in Table 2. (i) Only gray image, (ii) Gray image + R, (iii) Gray + R + G, (iv) Gray + R + G + B, (v) Gray + R + G + B + MSE, (vi) Gray + R + G + B + MSE + PSNR, (vii) Gray + R + G + B + MSE + PSNR + SSIM, (viii) Gray + R + G + B + MSE + PSNR + SSIM + High cluster, (ix) Gray + R + G + B + MSE + PSNR + SSIM + High cluster + Low cluster. Furthermore, new experiments were conducted to show that K = 2 is feasible for the classification of fruits and leaves infected by bacteria, viruses, and fungi. The classification rate was calculated for different K values. It can be observed from the table that K = 2 is feasible. This is valid because high values for healthy images and low values for diseased images are expected to be due to the distortion caused by black dots, yellow, and white patches. When we examine the results of each experiment listed in Table 2, the average classification rate increases gradually as additional steps are added to the previous step. Therefore, it is clear from this experiment that each step contributes equally to achieving the best results using the proposed method.

Table 2
Average classification rate of each component of the proposed method on our dataset

#	Steps	Fruit	Leaf
(i)	Only gray image	66.66	76.19
(ii)	Gray + R image	62.96	72.73
(iii)	Gray + R + G image	64.99	74.24
(iv)	Gray + R + G + B image	63.64	73.03
(v)	Gray + R + G + B image + MSE	78.56	83.76
(vi)	Gray + R + G + B image + MSE + PSNR	89.29	83.33
(vii)	Gray + R + G + B image + MSE + PSNR + SSIM	90.81	95.55
(viii)	Gray + R + G + B image + MSE + PSNR + SSIM + High cluster	13.64	18.75
(ix)	Gray + R + G + B image + MSE + PSNR + SSIM + Low cluster	22.73	25.00
(x)	Gray + R + G + B image + MSE + PSNR + SSIM + High cluster + Low cluster	90.81	95.55
(xi)	K = 2 for clustering	90.81	95.55
(xii)	K =3 for clustering	63.33	83.89
(xiii)	K = 4 for clustering	54.44	70.28
(xiv)	K = 5 for clustering	57.78	80.56
(xv)	**Proposed method**	**90.81**	**95.55**

It is noted from the Ablations study experiments in Table 2 that when we add quality measure features to different color spaces, the average classification rate jumps to more than 90% from 89% for fruits and 83% to 95% for leaves. Therefore, one can conclude that the combination of quality measure-based features and a dense network for classification is the best for achieving high classification results. This makes sense because the features extracted through quality measures are generic for the classification of affected images.

To show that the proposed model is effective compared to the standard CNN, we conducted new experiments using a standard CNN with different components of the proposed method. The results are reported in Table 3, where the standard CNN achieves the lowest accuracy, confirming that pixel-level features alone are insufficient. Adding the quality-metric branch produces a notable improvement, showing that MSE, PSNR, and SSIM features capture structural information essential for distinguishing disease patterns. When the fusion layer is introduced, performance increases further, indicating the complementary nature of CNN and quality-metric features. The complete proposed architecture achieves the highest accuracy across both fruit and leaf datasets, validating that every added component strengthens the model and collectively leads to superior classification. This shows that the standard CNN alone is not sufficient to address the challenge of fruit and leaf disease classification.

4.3. Experiments for classification on proposed dataset

Tables 4–6 report the quantitative results of the proposed method and existing approaches for classifying fruit and leaf samples infected by bacteria, viruses, and fungi, including methods proposed in Cao et al. [25], Chandrashekar et al. [11], Du et al. [36], Linfeng et al. [37], Sultana et al. [6], and Thakur et al. [30]. According to Tables 3–6, the proposed approach outperforms all existing approaches [6, 11, 25, 30, 36, 37] in terms of the average classification rate. Consequently, it can be concluded that the proposed approach is better than the existing approaches. The derived characteristics are robust to changes in the images and invariant to multiple domains (fruit and leaf), which is the primary reason why the proposed method produces better results. However, the scope of the methods in existing studies [6, 11, 25, 30, 36, 37] is limited to a specific dataset. Furthermore, fruit- and leaf-infected images cannot be successfully classified using these approaches because their effectiveness is dependent on the number of training samples. Because there were not enough examples in our dataset, we chose the number of training and testing samples using 10-fold cross-validation. Compared with the proposed method, the existing approaches perform poorly and lack the capacity for generalization. Nonetheless, as demonstrated by the ablation study trials, the crucial actions suggested in this study were successful and helped provide excellent outcomes. CNN and feature extraction work together to improve generalization, and the suggested approach outperforms the current approaches in terms of the average classification rate for both fruit and leaf datasets.

4.4. Experiments for classification on benchmark datasets

As mentioned earlier, each class of the proposed dataset contained samples of mixed items, but there was no class containing only fruits and leaves in our dataset. These datasets included fruits, leaves, stems, and vegetables affected by viruses, bacteria, and fungi in each class. In

Table 3
Average classification rate for the ablation study comparing the standard CNN with progressively enhanced versions of the proposed architecture

Steps	Fruit	Leaf
Baseline CNN + proposed classification	29.63	44.44
Image + SE (squeeze-and-excitation) + CNN + proposed classification	33.33	33.33
CSV only + CNN + proposed classification	33.24	40.0
Fusion no SepConv (CNN + CSV fusion is used, but WITHOUT the separable convolution) + proposed classification	42.50	33.33
Fusion no SE (CNN features and CSV features but without the SE/structural enhancement) + proposed classification	47.31	40.28
Proposed method -Fusion (CNN image features + CSV quality-metric features)	**90.81**	**95.55**

Table 4
Confusion matrix and ACR of the proposed and comparative methods on fruit and leaf disease pathogen classification (in %) B-Bacteria, F-Fungus and V-Virus

Fruit/ leaf class	Proposed						Chandrashekar et al. [11]						Sultana et al. [6]					
	Fruits			Leaf			Fruits			Leaf			Fruits			Leaf		
	B	F	V	B	F	V	B	F	V	B	F	V	B	F	V	B	F	V
Bacteria	91.20	4.80	4.00	95.00	3.75	1.25	86.80	7.50	5.70	89.17	5.83	5.00	82.80	8.40	8.80	84.17	10.42	5.42
Fungus	4.35	91.74	3.91	0.42	96.25	3.33	3.78	88.09	8.13	1.67	91.67	6.67	5.22	86.52	8.26	8.75	85.42	5.83
Virus	6.05	3.95	90.00	4.12	0.39	95.49	9.05	7.48	83.47	4.51	2.55	92.94	11.05	8.42	80.53	5.69	4.51	89.80
ACR		90.81			95.55			86.12			91.72			82.79			87.37	

Table 5
Confusion matrix and ACR of comparative methods on fruit and leaf disease pathogen classification (in %) B-Bacteria, F-Fungus and V-Virus

Fruit/ leaf class	Du et al. [36]						Linfeng et al. [37]					
	Fruits			Leaf			Fruits			Leaf		
	Bacteria	Fungus	Virus	Bacteria	Fungus	Virus	Bacteria	Fungus	Virus	Bacteria	Fungus	Virus
Bacteria	66.67	33.33	0	0	37.5	62.5	66.67	0	33.33	83.33	16.67	0
Fungus	0	100	0	0	60	40	66.67	0	33.33	0	100	0
Virus	20	40	40	0	0	100	50	0	50	0	100	0
ACR		63.64			60.00			38.89			61.11	

Table 6
Confusion matrix and ACR of additional comparative methods on fruit and leaf disease pathogen classification (in %) B-Bacteria, F-Fungus and V-Virus

Fruit/ leaf class	Thakur et al. [30]						Cao et al. [25]					
	Fruit			Leaf			Fruit			Leaf		
	Bacteria	Fungus	Virus	Bacteria	Fungus	Virus	Bacteria	Fungus	Virus	Bacteria	Fungus	Virus
Bacteria	20.00	5.00	5.00	96.5	2.00	0	25.00	16.70	13.33	51.00	44.00	5.00
Fungus	2.00	10.00	3.00	23.00	78.25	0	0	82.00	18.00	2.00	91.00	7.00
Virus	4.00	6.00	20.00	0	6.00	94.75	0	10.00	70.50	10.00	7.00	54.25
ACR		16.67			89.8			59.17			65.42	

other words, each class can have any type of image rather than each class for each type of image. In addition, the images are exposed to environmental conditions that affect their contents. Therefore, these two datasets are appropriate for confirming the robustness and capacity for generalization of the proposed method. Tables 7–9 show the performance of the proposed method and existing approaches on the two benchmark datasets in terms of the confusion matrix and average classification rates, including comparisons with recent state-of-the-art methods [25, 11, 36, 37, 6, 30]. Compared to the existing approaches, Tables 7–9 demonstrate that it obtained the best ACR for both datasets. This outcome suggests that the proposed approach is highly robust and has good generalization capabilities. Better results were obtained for

Table 7
Confusion matrix and ACR of the proposed and comparative methods on the NZDLPlantDisease-v1 and NZDLPlantDisease-v2 datasets (in %) B-Bacteria, F-Fungus, H-Health and V-Virus

F/L class	Proposed								Chandrashekar et al. [11]								Sultana et al. [6]							
	NZDLPlant-v1				NZDLPlant-v2				NZDLPlant-v1				NZDLPlant-v2				NZDLPlant-v1				NZDLPlant-v2			
	B	F	H	V	B	F	H	V	B	F	H	V	B	F	H	V	B	F	H	V	B	F	H	V
Bacteria	92.4	3.28	2.15	2.09	92.0	2.27	3.19	2.48	87.6	4.78	4.27	3.27	87.2	4.91	4.36	3.44	86.9	4.14	5.24	3.66	85.9	4.36	5.24	4.46
Fungus	3.57	90.2	3.25	2.98	2.73	89.6	4.05	3.54	5.07	86.9	3.90	4.11	5.86	85.1	4.70	4.29	3.86	85.0	5.94	5.19	5.73	82.4	6.44	5.40
Health	3.54	2.62	91.9	1.86	2.35	2.55	91.0	4.04	4.72	4.60	87.8	2.78	4.77	4.63	87.6	2.85	4.19	4.49	85.2	6.10	5.20	5.29	83.2	6.25
Virus	4.05	3.17	2.50	90.2	2.95	3.28	3.19	90.5	4.91	3.88	3.51	87.7	4.93	3.88	3.59	87.6	4.97	3.56	5.48	85.9	6.00	5.13	5.48	83.3
ACR	**91.23**				**90.84**				87.53				86.78				85.79				83.75			

Table 8
Confusion matrix and ACR of comparative methods on benchmark datasets (in %) B-Bacteria, F-Fungus, H-Health and V-Virus

	Du et al. [36]								Linfeng et al. [37]							
	NZDLPlant-v1				NZDLPlant-v2				NZDLPlant-v1				NZDLPlant-v2			
F/L class	**B**	**F**	**H**	**V**	**B**	**F**	**H**	**V**	**B**	**F**	**H**	**V**	**B**	**F**	**H**	**V**
Bacteria	68.75	1.92	1.44	27.88	29.33	15.87	54.81	0	85.86	2.09	0	12.04	19.9	0	61.78	18.32
Fungus	0	100	0	0	0	100	0	0	19.35	80.65	0	0	19.35	12.9	58.06	9.68
Health	32	0	52.8	15.2	0	2.40	97.60	0	66.67	1.42	9.93	21.99	0	0	95.74	4.26
Virus	0	0	0	100	2.67	2.45	36.75	58.13	1.79	0	0	98.21	1.12	0	4.91	93.97
ACR	85.84				61.42				68.66				55.63			

Table 9
Confusion matrix and ACR of additional comparative methods on benchmark datasets (in %) B-Bacteria, F-Fungus, H-Health and V-Virus

	Thakur et al. [30]								Cao et al. [25]							
	NZDLPlant-v1				NZDLPlant-v2				NZDLPlant-v1				NZDLPlant-v2			
F/L class	**B**	**F**	**H**	**V**	**B**	**F**	**H**	**V**	**B**	**F**	**H**	**V**	**B**	**F**	**H**	**V**
Bacteria	0.56	0.00	0.00	99.44	0	0	0	100	53.51	14.59	16.22	15.68	70.27	3.78	20.00	5.95
Fungus	0.00	0.00	0.00	100	0	0	0	100	6.93	88.12	4.95	0	18.81	66.34	10.89	3.96
Health	0.00	0.00	0.00	100	0	0	0	100	26.39	9.03	58.33	6.25	33.33	4.17	52.78	9.72
Virus	0.00	00.0	0.00	100	2.67	0	0	100	2.47	0	0	97.53	0.22	0	0	99.78
ACR	25.14				25.00				74.87				72.79			

the benchmark datasets when we compared the performance of the proposed strategy on the collected dataset (for this study) with that on the benchmark datasets. The primary explanation is that the combination of quality metrics and image-based features with CNN preserves significant image information because the benchmark datasets contain high-quality images. The performance of the proposed approach is superior to that of the current methods, as shown in Tables 7–9. This is evident because existing methods are developed to address a specific challenge, but not multiple domains, such as fruits and leaves.

The average classification rates of the proposed and current approaches, which are shown in Table 10 for both fruit and leaf-infected images for classification, support these conclusions. Table 10 shows that the outcomes of Chandrashekar et al. [11] are comparable to those of the proposed method. This is because the approach was created for the classification of diseases in mango leaves, whereas Sultana et al. [6] offered a separate method for other fruits that is not for disease classification. However, when compared to the suggested and other existing approaches, Saleem et al. [34, 35] obtained high results for NZDLPlantDisease-v1 and NZDLPlantDisease-v2, respectively, for the two benchmark datasets. This is because these two approaches were created to tackle the difficulties presented by the two datasets. Given the small disparity, this finding may not be considered a significant flaw. In comparison to the current approaches, it is also observed that the proposed approach produces findings for every trial that are nearly identical. Therefore, unlike existing methods, the proposed method is ideal for real-time applications because it is stable, dependable, and domain-independent (fruit and leaf domains). The findings of Saleem et al. [34] and Saleem et al. [35] were used for comparison. However, we used them to compute measures for comparison with other approaches currently in use [6, 11, 25, 30, 36, 37].

Table 10
The mean average precision of the proposed and existing methods on fruit and leaf of our dataset and two benchmark datasets (in %)

	Our dataset			
Method	**Fruit class**	**Leaf class**	**NZDLPlantDisease-v1**	**NZDLPlantDisease-v2**
Proposed method	**90.99**	**95.58**	91.23	90.84
Chandrashekar et al. [11]	86.12	91.33	87.57	86.97
Sultana et al. [6]	83.27	86.45	85.82	83.76
Saleem et al. [34]	-	-	93.80	-
Saleem et al. [35]	-	-	87.68	91.33
Du et al. [36]	83.86	83.04	90.59	82.97
Linfeng et al. [37]	57.03	65.79	87.49	83.11
Thakur et al. [30]	18.56	89.24	28.65	28.34
Cao et al. [25]	68.53	89.97	77.19	75.23

Table 11
Performance comparison of the proposed and state-of-the-art methods on two external benchmark datasets

	Augmented Grapevine Disease				Plant Disease Recognition			
Methods	**Accuracy**	**Precision**	**Recall**	**F-score**	**Accuracy**	**Precision**	**Recall**	**F-score**
Proposed method	**77.17**	**83.00**	**85.00**	**83.00**	**80.40**	**80.37**	**81.72**	**80.27**
Chandrashekar et al. [11]	68.90	65.34	68.67	70.21	59.89	61.00	58.42	61.16
Sultana et al. [6]	59.54	57.89	55.20	60.30	69.50	67.42	64.40	66.36
Du et al. [36]	66.00	63.46	65.88	66.28	79.00	77.21	75.33	71.87
Linfeng et al. [37]	72.00	68.28	78.00	79.40	39.56	25.77	39.56	27.33
Thakur et al. [30]	28.50	64.57	29.00	17.90	33.33	11.11	11.11	11.11
Cao et al. [25]	75.12	79.57	83.89	80.43	78.22	77.67	79.34	75.45

Table 12
ACR of the proposed and existing methods for the leave-one-class-out validation dataset on fruit and leaf diseases

Training classes	Testing classes	Proposed		Chandrashekar et al. [11]		Sultana et al. [6]		Du et al. [36]		Linfeng et al. [37]	
		Fruit	**Leaf**	**Fruit**	**Leaf**	**Fruit**	**Leaf**	**Fruit**	**Leaf**	**Fruit**	**Leaf**
Bacteria	Fungus, virus	**83.25**	**88.20**	80.85	86.00	78.23	84.70	78.40	75.41	27.57	31.16
Virus	Bacteria, fungus	**86.32**	**90.71**	84.23	87.21	81.12	86.71	50.00	50.38	49.68	51.88
Fungus	Bacteria, virus	**81.68**	**85.33**	80.28	83.94	78.53	80.23	41.18	45.71	36.73	38.94

To show that the proposed method is generic and reliable, we also evaluated the proposed and existing methods on two different datasets, namely the Plant Disease Recognition and Augmented Grapevine Disease Datasets [38] using Accuracy (A), Precision (P), Recall (R), and F-score (F) on two external benchmark datasets—Augmented Grapevine Disease and Plant Disease Recognition. These metrics offer deeper insight into the reliability, sensitivity, and specificity of each model under diverse disease types and imaging conditions. The results, shown in Table 11, demonstrate that the proposed method achieves the best overall balance across all four metrics compared with existing techniques. Therefore, one can infer that the features extracted are robust and effective for successful classification, while due to inherent limitations, such as focusing on a specific dataset and a lack of generic nature in feature extraction, the existing methods do not perform well compared to the proposed method.

4.5. Experiments to analyze robustness

As shown in Tables 12 and 13, we conducted leave-one-class-out validation, along with experiments under different scaling, rotations, Gaussian blur, noise, and cross-dataset settings, to evaluate the reliability, efficiency, and domain independence of the proposed approach and to compare it with existing methods [25, 11, 36, 37, 6, 30]. For the fruit and leaf datasets, the leave-one-class-out validation tests showed that the proposed model was resilient across several disease pathogen classes (Tables 12 and 13). This validation method offers important information about the model's capacity to recognize disease types, even in cases where one class is completely disregarded during training. As indicated in Tables 12 and 13, the same conclusions can be drawn based on the results of the current approaches. Compared with the current methods, the experiments listed in Table 14 demonstrate that the proposed method produces nearly consistent results for various scales, rotations, blurs, and noises. This suggests that the approach proposed in this study is unaffected by noise, blur, rotation, or scale. This illustrates the benefits of using a basic CNN-based classifier in conjunction with feature extraction methods. According to a summary of the findings, the proposed approach is efficient, domain-independent, noise-resistant, and invariant to various rotations, scaling, blurring, and noise.

Table 13
ACR of the existing methods for the leave-one-class-out validation dataset on fruit and leaf diseases

Training classes	Testing classes	Thakur et al. [30]		Cao et al. [25]	
		Fruit	**Leaf**	**Fruit**	**Leaf**
Bacteria	Fungus, virus	48.28	80.41	0	10.00
Virus	Bacteria, fungus	2.44	0	0	0
Fungus	Bacteria, virus	76.30	50.00	0	0

4.6. Experiments for domain independence

To further demonstrate the domain independence of the proposed model, cross-domain experiments are conducted by training the model on one crop type (fruit) and testing it on another (leaf), and vice versa. The results presented in Table 15 show a clear performance advantage of the proposed method compared to existing approaches across both cross-domain settings. This is evident that the proposed method is domain independent, while the existing methods are not.

Despite its strong performance, several limitations remain. The method may face challenges when processing images with overlapping disease symptoms, mixed-pathogen infections, or extreme variations in illumination and background complexity. Addressing these limitations requires exploring more advanced feature-fusion techniques, incorporating temporal information from progressive infection stages, and extending training to larger, more diverse datasets. Future work will also focus on enhancing model interpretability and developing an optimized version for embedded hardware. These improvements will

Table 14
The average classification rate of the proposed and existing methods on scaled, rotated, and distorted images

	Random scaling up and down		Random rotations		Different levels of Gaussian noise		Different levels of Gaussian blur	
Methods	**Fruit**	**Leaf**	**Fruit**	**Leaf**	**Fruit**	**Leaf**	**Fruit**	**Leaf**
Proposed method	**90.53**	**95.55**	**89.02**	**95.50**	**90.44**	**88.55**	**91.88**	**85.19**
Chandrashekar et al. [11]	85.98	91.12	86.12	91.72	33.33	35.34	33.33	33.33
Sultana et al. [6]	82.02	87.34	82.79	87.37	59.09	12.00	63.64	32.00
Linfeng et al. [37]	33.33	76.60	33.33	38.89	33.33	33.33	33.33	38.89
Thakur et al. [30]	43.16	93.33	35.90	94.10	61.90	33.33	66.67	20.83
Cao et al. [25]	42.86	76.19	60.05	93.51	61.11	78.57	48.15	58.33

Table 15
The average classification rate of the proposed and existing methods for cross-domain experiments on fruit and leaf datasets

Training dataset	Testing dataset	Proposed method	Chandrashekar et al. [11]	Sultana et al. [6]	Du et al. [36]	Linfeng et al. [37]	Thakur et al. [30]	Cao et al. [25]
Fruit	Leaf	**89.54**	26.04	40.70	27.42	52.42	40.30	35.48
Leaf	Fruit	**93.30**	40.91	45.52	35.19	34.26	64.8	35.19

support broader and more reliable adoption of the proposed system in real-world agricultural applications.

As shown in Figure 12, the proposed approach performs poorly on images with significant noise and degradation but is resilient to unfavorable circumstances. Furthermore, the proposed approach cannot work effectively if the same photos are affected by several factors, such as if the image contains visual indicators of multiple disease pathogens. For example, in Figure 12, the proposed approach misclassified a fungal image as a bacterial one. Initially, bacterial infections manifest as black spots, which are subsequently overgrown by fungal infections, appearing as white patches. This overlap of features in the affected regions poses a challenge for the classifier because it may incorrectly attribute the combined visual characteristics to a single class. However, this is beyond the scope of the present study. This limitation can be overcome by proposing a segmentation step that separates the regions of interest of different disease pathogens, and the segmented region can then be analyzed further to classify the images. Hence, instead of using global information in the proposed approach, local information can be used to address the above challenges in future studies.

Figure 12
Example of failure cases caused by overlapping disease symptoms in fruit and leaf images

Fungus - Bacteria Bacteria - Fungus

5. Conclusion and Future Work

In this study, we proposed a novel approach for the classification of fruit and leaf diseases by integrating quality-metric features with a lightweight CNN to achieve domain-independent and robust performance. For the input of Gray, R, G, and B images, the connected component approach is used for detecting patches through K-means clustering with K = 2. The feature-based quality measures are extracted from the connected components. To improve the discriminative power of the features, we also extracted visual features from the input images directly using CNN. The quality measures based on features and visual features are fused and fed to the dense network for classification. Experimental results on our dataset and benchmark datasets show that the proposed method is the best in terms of average classification rate compared to the state-of-the-art methods which proves the robustness of the proposed method. To further demonstrate consistency in the performance of the proposed method, experiments are conducted on different rotations, scaling, noise, and blurred images. Further, cross-domain validation experiments are conducted to show that the proposed method is generic and domain-independent.

The proposed framework can be integrated into mobile devices, handheld imaging tools, and edge-computing platforms to enable real-time, on-field diagnostics for farmers. Such deployment would reduce reliance on high-computing resources and make the system suitable for agricultural environments with limited connectivity.

Ethical Statement

This study does not contain any studies with human or animal subjects performed by any of the authors.

Conflicts of Interest

Palaiahnakote Shivakumara is the Editor-in-Chief for Artificial Intelligence and Applications, and he is not involved in the editorial review or the decision to publish this article. The authors declare that they have no conflicts of interest to this work.

Data Availability Statement

Data sharing is not applicable to this article as no new data were created or analyzed in this study.

Author Contribution Statement

Poornima Basatti Hanuma Gowda: Conceptualization, Software, Data curation, Writing – original draft, Visualization. **Basavanna Mahadevappa:** Formal analysis, Investigation, Supervision, Project administration. **Shivakumara Palaiahnakote:** Methodology, Writing – review & editing. **Muhammad Hammad Saleem:** Validation. **Niranjan Mallappa Hanumanthu:** Resources.

References

[1] Liu, J., & Wang, X. (2021). Plant diseases and pests detection based on deep learning: A review. *Plant Methods*, *17*(1), 22. https://doi.org/10.1186/s13007-021-00722-9

[2] Jiang, P., Chen, Y., Liu, B., He, D., & Liang, C. (2019). Real-time detection of apple leaf diseases using deep learning approach based on improved convolutional neural networks. *IEEE Access*, *7*, 59069–59080. https://doi.org/10.1109/ACCESS.2019.2914929

[3] Prajwala, M., Kumar, P. P., Gopinath, S. M., Palaiahnakote, S., Basavanna, M., & Lopresti, D. P. (2025). Domain-independent adaptive histogram-based features for pomegranate fruit and leaf diseases classification. *CAAI Transactions on Intelligence Technology*, *10*(2), 317–336. https://doi.org/10.1049/cit2.12390

[4] Abbas, S., Khan, M. A., Alhaisoni, M., Tariq, U., Armghan, A., Alenezi, F., ... & Thinnukool, O. (2023). Crops leaf diseases recognition: A framework of optimum deep learning features. *Computers, Materials & Continua*, *74*(1). 1139–1159. http://dx.doi.org/10.32604/cmc.2023.028824

[5] Iftikhar, M., Kandhro, I. A., Kausar, N., Kehar, A., Uddin, M., & Dandoush, A. (2024). Plant disease management: A fine-tuned enhanced CNN approach with mobile app integration for early detection and classification. *Artificial Intelligence Review*, *57*(7), 167. https://doi.org/10.1007/s10462-024-10809-z

[7] Bansal, P., Kumar, R., & Kumar, S. (2021). Disease detection in apple leaves using deep convolutional neural network. *Agriculture*, *11*(7), 617. https://doi.org/10.3390/agriculture11070617

[6] Sultana, S., Tasir, M. A. M., Nobel, S. N., Kabir, M. M., & Mridha, M. F. (2024). XAI-FruitNet: An explainable deep model for accurate fruit classification. *Journal of Agriculture and Food Research*, *18*, 101474. https://doi.org/10.1016/j.jafr.2024.101474

[8] Anim-Ayeko, A. O., Schillaci, C., & Lipani, A. (2023). Automatic blight disease detection in potato (Solanum tuberosum L.) and tomato (Solanum lycopersicum, L. 1753) plants using deep learning. *Smart Agricultural Technology*, *4*, 100178. https://doi.org/10.1016/j.atech.2023.100178

[9] Mallikarjuna, S. B., Shivakumara, P., Khare, V., Basavanna, M., Pal, U., & Poornima, B. (2022). Multi-gradient-direction based deep learning model for arecanut disease identification. *CAAI Transactions on Intelligence Technology*, *7*(2), 156–166. https://doi.org/10.1049/cit2.12088

[10] Javidan, S. M., Banakar, A., Rahnama, K., Vakilian, K. A., & Ampatzidis, Y. (2024). Feature engineering to identify plant diseases using image processing and artificial intelligence: A comprehensive review. *Smart Agricultural Technology*, *8*, 100480. https://doi.org/10.1016/j.atech.2024.100480

[11] Chandrashekar, C., Vijayakumar, K. P., Pradeep, K., & Balasundaram, A. (2024). MDCN: Modified dense convolution network based disease classification in Mango leaves. *Computers, Materials and Continua*, *78*(2), 2511–2533. http://dx.doi.org/10.32604/cmc.2024.047697

[12] Li, W., Yu, X., Chen, C., & Gong, Q. (2023). Identification and localization of grape diseased leaf images captured by UAV based on CNN. *Computers and Electronics in Agriculture*, *214*, 108277. https://doi.org/10.1016/j.compag.2023.108277

[13] Liu, Y., Wang, Z., Wang, R., Chen, J., & Gao, H. (2023). Flooding-based MobileNet to identify cucumber diseases from leaf images in natural scenes. *Computers and Electronics in Agriculture*, *213*, 108166. https://doi.org/10.1016/j.compag.2023.108166

[14] Li, Y., Wang, J., Wu, H., Yu, Y., Sun, H., & Zhang, H. (2022). Detection of powdery mildew on strawberry leaves based on DAC-YOLOv4 model. *Computers and Electronics in Agriculture*, 202, 107418. https://doi.org/10.1016/j.compag.2022.107418

[15] Liu, B., Huang, X., Sun, L., Wei, X., Ji, Z., & Zhang, H. (2024). MCDCNet: Multi-scale constrained deformable convolution network for apple leaf disease detection. *Computers and Electronics in Agriculture*, *222*, 109028. https://doi.org/10.1016/j.compag.2024.109028

[16] Thakkar, S., Patel, C., & Suthar, V. (2023). Plant disease identification using machine learning and image processing. *ICTACT Journal on Soft Computing*, *13*(4), 3043–3047. https://doi.org/10.21917/ijsc.2023.0428

[17] Thai, H. T., Le, K. H., & Nguyen, N. L. T. (2023). FormerLeaf: An efficient vision transformer for Cassava Leaf Disease detection. *Computers and Electronics in Agriculture*, *204*, 107518. https://doi.org/10.1016/j.compag.2022.107518

[18] Pradhan, P., Kumar, B., Kumar, K., & Bhutiani, R. (2024). Plant disease detection using leaf images and an involutional neural network. *Environment Conservation Journal*, *25*(2), 452–462. https://doi.org/10.36953/ECJ.28142024

[19] Rani, L., Sarangi, P. K., & Sahoo, A. K. (2024). Image-feature based deep learning model for plant leaf disease detection. *Macromolecular Symposia*, *413*(1), 2200216. https://doi.org/10.1002/masy.202200216

[20] Vásconez, J. P., Vásconez, I. N., Moya, V., Calderón-Díaz, M. J., Valenzuela, M., Besoain, X., ... & Cheein, F. A. (2024). Deep learning-based classification of visual symptoms of bacterial wilt disease caused by Ralstonia solanacearum in tomato plants. *Computers and Electronics in Agriculture*, *227*, 109617. https://doi.org/10.1016/j.compag.2024.109617

[21] Chin, P.-W., Ng, K.-W., & Palanichamy, N. (2024). Plant disease detection and classification using deep learning methods: A comparison study. *Journal of Informatics and Web Engineering*, *3*(1), 155–168. https://doi.org/10.33093/jiwe.2024.3.1.10

[22] Khanal, B., Poudel, P., Chapagai, A., Regmi, B., Pokhrel, S., & Khanal, S. R. (2024). Paddy disease detection and classification using computer vision techniques: A mobile application to detect paddy disease. *arXiv Preprint:2412.05996*. https://doi.org/10.48550/arXiv.2412.05996

[23] Benfenati, A., Causin, P., Oberti, R., & Stefanello, G. (2023). Unsupervised deep learning techniques for automatic detection of plant diseases: Reducing the need of manual labelling of plant images. *Journal of Mathematics in Industry*, *13*(1), 5. https://doi.org/10.1186/s13362-023-00133-6

[24] Thakur, P. S., Khanna, P., Sheorey, T., & Ojha, A. (2022). Explainable vision transformer enabled convolutional neural network for plant disease identification: PlantXViT. *arXiv Preprint:2207.07919*. https://doi.org/10.48550/arXiv.2207.07919

[25] Cao, K., Yang, Y., Xu, L., Wan, X., Yang, L., & Jia, W. (2025). GAF-Net: An enhanced multidisease for corn leaves detection model based on YOLOv8. *IEEE Transactions on AgriFood Electronics*, *3*(2), 420–432. https://doi.org/10.1109/TAFE.2025.3561196

[26] Pacal, I., Kunduracioglu, I., Alma, M. H., Deveci, M., Kadry, S., Nedoma, J., ... & Martinek, R. (2024). A systematic review of

deep learning techniques for plant diseases. *Artificial Intelligence Review*, *57*(11), 304. https://doi.org/10.1007/s10462-024-10944-7

[27] Tejaswini, Rastogi, P., Dua, S., Manikanta, & Dagar, V. (2024). Early disease detection in plants using CNN. *Procedia Computer Science*, *235*, 3468–3478. https://doi.org/10.1016/j.procs.2024.04.327

[28] Pandian, J. A., Kumar, V. D., Geman, O., Hnatiuc, M., Arif, M., & Kanchanadevi, K. (2022). Plant disease detection using deep convolutional neural network. *Applied Sciences*, *12*(14), 6982. https://doi.org/10.3390/app12146982

[29] Wang, Y., Wang, H., & Peng, Z. (2021). Rice diseases detection and classification using attention based neural network and bayesian optimization. *Expert Systems with Applications*, *178*, 114770. https://doi.org/10.1016/j.eswa.2021.114770

[30] Thakur, P. S., Chaturvedi, S., Seal, A., Khanna, P., Sheorey, T., & Ojha, A. (2025). An Ultra lightweight interpretable convolution-vision transformer fusion model for plant disease identification: ConViTX. *IEEE Transactions on Computational Biology and Bioinformatics*, *22*(1), 310–321. https://doi.org/10.1109/TCBBIO.2024.3515149

[31] Kumar, K., Tripathi, K., & Gupta, R. (2023). Image based plant disease classification using deep learning technique. *International Journal of Innovative Research in Engineering and Management*, *10*(3), 146–151.

[32] Saraswat, S., Singh, P., Kumar, M., & Agarwal, J. (2024). Advanced detection of fungi-bacterial diseases in plants using modified deep neural network and DSURF. *Multimedia Tools and Applications*, *83*(6), 16711–16733. https://doi.org/10.1007/s11042-023-16281-1

[33] Uppal, A., Naruka, M. S., & Tewari, G. (2023). Image processing based plant disease detection and classification. *International Journal on Recent and Innovation Trends in Computing and Communication*, *11*(1s), 52–56. https://doi.org/10.17762/ijritcc.v11i1s.5993

[34] Saleem, M. H., Potgieter, J., & Arif, K. M. (2022). A performance-optimized deep learning-based plant disease detection approach for horticultural crops of New Zealand. *IEEE Access*, *10*, 89798–89822. https://doi.org/10.1109/ACCESS.2022.3201104

[35] Saleem, M. H., Potgieter, J., & Arif, K. M. (2022). A weight optimization-based transfer learning approach for plant disease detection of New Zealand vegetables. *Frontiers in Plant Science*, *13*, 1008079. https://doi.org/10.3389/fpls.2022.1008079

[36] Du, L., Zhu, J., Liu, M., & Wang, L. (2025). YOLOv7-PSAFP: Crop pest and disease detection based on improved YOLOv7. *IET Image Processing*, *19*(1), e13304. https://doi.org/10.1049/ipr2.13304

[37] Linfeng, W., Jiayao, L., Yong, L., Yunsheng, W., & Shipu, X. (2024). A lightweight tomato leaf disease identification method based on shared–twin neural networks. *IET Image Processing*, *18*(9), 2291–2303. https://doi.org/10.1049/ipr2.13094

[38] Panchananam, L. S., Chandaliya, P. K., Akhtar, Z., Upla, K., & Ramachandra, R. (2025). WaveletFusion: Enhancing plant leaf disease classification with multi-scale feature extraction and explainable AI. *Expert Systems with Applications*, *285*, 127947. https://doi.org/10.1016/j.eswa.2025.127947

How to Cite: Gowda, P. B. H., Mahadevappa, B., Palaiahnakote, S., Saleem, M. H., & Hanumanthu, N. M. (2026). A New Domain-Independent Approach for Classification of Bacteria, Fungus, and Virus-Infected Fruit and Leaf Images. *Artificial Intelligence and Applications*. https://doi.org/10.47852/bonviewAIA62027747